

NASA TECHNICAL NOTE



NASA TN D-2956

C. 1

NASA TN D-2956

LOAN COPY: RE
APVL (V)
KIRTLAND AFB

0079953

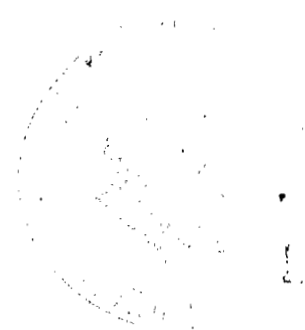


TECH LIBRARY KAFB, NM

STUDIES RELATING TO THE ATTAINMENT OF HIGH LIFT-DRAG RATIOS AT HYPERSONIC SPEEDS

*by David E. Fetterman, Arthur Henderson, Jr.,
Mitchel H. Bertram, and Patrick J. Johnston*

*Langley Research Center
Langley Station, Hampton, Va.*



c-1

ERRATA

NASA Technical Note D-2956

STUDIES RELATING TO THE ATTAINMENT OF HIGH
LIFT-DRAG RATIOS AT HYPERSONIC SPEEDS

By David E. Fetterman, Arthur Henderson, Jr.,
Mitchel H. Bertram, and Patrick J. Johnston
August 1965

Page 28: Replace figure 12 with attached figure 12, in which the $(L/D)_{max}$ data originally given for the rectangular cross section (center graph) have been significantly altered to correct for recently discovered data-reduction errors.

*Completed
m B
1 Dec 65*



STUDIES RELATING TO THE ATTAINMENT OF HIGH
LIFT-DRAG RATIOS AT HYPERSONIC SPEEDS

By David E. Fetterman, Arthur Henderson, Jr.,
Mitchel H. Bertram, and Patrick J. Johnston

Langley Research Center
Langley Station, Hampton, Va.

NATIONAL AERONAUTICS AND SPACE ADMINISTRATION

For sale by the Clearinghouse for Federal Scientific and Technical Information
Springfield, Virginia 22151 - Price \$2.00

STUDIES RELATING TO THE ATTAINMENT OF HIGH
LIFT-DRAG RATIOS AT HYPERSONIC SPEEDS*

By David E. Fetterman, Arthur Henderson, Jr.,
Mitchel H. Bertram, and Patrick J. Johnston
Langley Research Center

SUMMARY

An evaluation of results of recent investigations of slender configurations to determine factors having the most significant influence on aerodynamic efficiency is presented. The results, which were obtained at a Mach number of 6.8 in air and of 20 in helium, show the effects on maximum lift-drag ratio of viscosity, body longitudinal curvature, cross-sectional shape, and fineness ratio, wing location, planform leading-edge sweep and diameter, and volumetric efficiency. In addition, the interrelationship of these factors in determining the extent of beneficial effects from favorable interference is examined. Included also are preliminary comparisons between certain merged wing-body configurations and discrete wing-body types.

INTRODUCTION

In applications to air-breathing hypersonic flight such as that for recoverable boosters, hypersonic transports, and reconnaissance aircraft where range is of primary interest, the need for high-lift-drag-ratio capability needs little justification. For military systems with reentry capability, the lift-drag ratio has a smaller effect on range but is still of interest for better maneuvering and trajectory control capability. Aerodynamic principles for providing these high lift-drag ratios at hypersonic speeds are not clear at present because, in contrast with the extensive effort that has been applied to blunt shapes for space and missile applications, research results on efficient hypersonic shapes are scarce.

As a help in establishing these hypersonic aerodynamic principles an experimental program is being pursued at the Langley Research Center. The scope of the initial phase of the program is indicated in figure 1. In this phase only

*Some of the material presented in this report was originally presented at the AIAA Military Aircraft Systems and Technology Meeting at Washington, D.C., September 21-23, 1964.

simple configurations of the major lifting elements - the body and wing - are being treated. The three classes shown cover the configuration spectrum. Lifting bodies are of interest because they combine large internal volume with small surface area and are structurally compact. Discrete wing-bodies possess potentially favorable interference benefits and may have better characteristics at landing speeds. Merged wing-bodies tend to combine the features of both classes. The drawings shown in figure 1 are not intended to indicate the exact models tested but rather to show, in a general way, the variations covered. These variations include body longitudinal curvature and cross-sectional shape, wing planform and leading-edge position. The models were tested in the position shown and also inverted to determine their optimum attitude. Investigations were conducted in the Langley 11-inch hypersonic tunnel at Mach numbers of 6.8 and 9.7 in air at stagnation temperatures of 1110° R and 1600° R, respectively, and in the Langley 22-inch helium tunnel at a Mach number of 20 at a stagnation temperature of 540° R. Maximum lift-drag ratios obtained from these investigations comprise the substance of this paper. These lift-drag ratios have been corrected to the condition where free-stream pressure exists on the body base. Reference 1 contains some of the unclassified results of this paper; however, portions of the helium data are somewhat different from the data presented here. The difference is due to the effects of base pressure for which data were not available at the time reference 1 was prepared.

SYMBOLS

A	local cross-sectional area of body
A_b	body base area
A_c	local cross-sectional area of cone
a	distance from body apex to body-wing intersection
b	body width
b'	semispan of exposed wing
C	coefficient in linear viscosity law
$C_{p,c}$	pressure coefficient on cone
$C_{p,o}$	pressure coefficient on cone windward ray
$C_{p,WB}$	pressure coefficient at wing-body juncture
c	wing chord
c_r	wing root chord
c_t	wing tip chord

d	wing-leading-edge diameter
$d_e \equiv 2\sqrt{A_b/\pi}$	
F	body fineness ratio, L/d_e
h	body height
L	length of wing or body
$(L/D)_{MAX}$	maximum value of lift-drag ratio
M	free-stream Mach number
n	exponent in power-law profile shape
p	free-stream pressure
p_l	local pressure
R_L	Reynolds number based on free-stream conditions and L
r_b	base radius of body
r_l	local radius of body
S_p	total planform area
S_w	exposed wing area
S_{ws}	wing area covered by body shock
s	lateral surface distance on configuration measured from midline of body
s_o	lateral surface distance on configuration from midline of body to wing edge
t/c	ratio of wing thickness to chord length
V	configuration volume
x	distance from body apex along longitudinal axis
y'	location of intersection of wing and body-shock measured from body in spanwise direction
α	angle of attack

$\alpha_{(L/D)_{MAX},FB}$ angle of attack for $(L/D)_{MAX}$ for flat-bottom configuration
 α_{SD} angle of attack for leading-edge shock detachment
 θ_c semivertex angle of cone
 Λ leading-edge sweep angle
 ϕ meridian angle measured from cone windward ray
 \bar{X} viscous interaction parameter, $\frac{M^3\sqrt{C}}{\sqrt{R_L}}$

Abbreviations:

FB flat-bottom configuration (body mounted above wing)
 FT flat-top configuration (body mounted below wing)

EFFECTS OF VISCOUS INTERACTION AND REYNOLDS NUMBER ON $(L/D)_{MAX}$

Since the ultimate attainable lift-drag ratio is given by the two-dimensional flat plate of zero thickness, it is appropriate to begin by considering the effects of viscosity on its performance. In Bertram's work (refs. 2 and 3) it was assumed that the boundary layer grew in the local inviscid flow behind the bow shock. With this approach it was found that the viscous effects on both lift and drag essentially canceled and the lift-drag ratio was relatively unaffected. White, however, (ref. 4) has shown the more nearly correct approach is to consider the flow over the plate to be displaced by both the angle of attack and the boundary layer. In this case, viscous interaction is found to affect the lift-drag ratio significantly. This is shown in figure 2 by results from a thin delta wing for a Mach number near 10. Shown are theoretical and experimental maximum lift-drag ratios obtained for a 2.5-percent-thick, 60° sweep delta wing at various Reynolds numbers based on root chord. The penalty produced on the wing lift-drag ratio by viscous interaction is readily seen.

Another point illustrated by these results and which is important to this paper is the large variation in lift-drag ratio caused by variations in Reynolds number. Meaningful comparisons of the lift-drag ratios of various configurations can therefore only be made at constant Reynolds number and similar boundary-layer conditions. Because constant Reynolds number results were not available at a Mach number of 9.7, subsequent results are limited to Mach numbers of 6.8 in air and 20 in helium. The majority of the air data at a Mach number of 6.8 are shown at a Reynolds number (based on length) of about 1.5×10^6 and the helium data at a Mach number of 20, at a Reynolds number of 3.5×10^6 . With these Reynolds numbers, predominantly laminar flow exists the

full length of the models. For these tests it was not possible to obtain constant Reynolds number conditions at the two Mach numbers and still retain overall laminar-boundary-layer conditions. For this reason and also because no attempt has been made to account for air-helium simulation effects, comparisons of the lift-drag-ratio level at the two Mach numbers will be avoided.

POINTED-BODY RESULTS

Figure 3 shows the maximum lift-drag characteristics of pointed body shapes at the two Mach numbers. The basis of comparison is the volume parameter $V^{2/3}/S_p$ where V is the volume and S_p is the total planform area. As this parameter decreases, the bodies become more slender. At a Mach number of 6.8 the data for half cones of semivertex angles of 3° to 10° (solid line represents flat side up and dashed line, flat side down) indicate that the flat side down gives better maximum lift-drag ratios at the higher cone angles. At lower cone angles the lifting efficiency of the round bottom (flat side up) is greatly reduced and its $(L/D)_{MAX}$ drops significantly below the flat-bottom version. The data for full cones indicate markedly superior characteristics for full cones at high values of the volume parameter. The half cones are penalized here because of large semivertex angles required to obtain high values of the volume parameter. At lower values of $V^{2/3}/S_p$ within the range of investigation, however, the full cones are clearly inferior.

The shaded areas in the data for a Mach number of 6.8 represent results obtained from power-law half bodies and also a half body of a minimum-drag profile constrained for volume and length as proposed by Miele (ref. 5). The results, which show general agreement with the half-cone results, indicate that longitudinal-curvature effects on $(L/D)_{MAX}$ are small. Results are also shown for triangular and square cross-section bodies and half-cone-cylinders. The square body and the flat-bottom cone-cylinder show some improvement in $(L/D)_{MAX}$ over the conical bodies.

At a Mach number of 20 in helium the flat-bottom half cone shows marked superiority over the flat-top half cone. Insufficient data exist to evaluate the relative merits of half and full cones; however, the data show qualitative agreement with that obtained at a Mach number of 6.8.

DELTA-WING RESULTS

Delta-wing results are presented at a Mach number of 6.8 in figure 4. The volume parameter $V^{2/3}/S_p$ is again used as a basis of comparison and, in contrast with the pointed bodies, the more highly swept the delta wing, the higher is the value of $V^{2/3}/S_p$. Data are shown for sharp leading-edge, symmetrical delta wings with maximum thickness at center chord and for unsymmetrical delta

wings with the maximum thickness at the trailing edge. Numbers indicate leading-edge sweep angles and, at constant sweep, the thickness ratio increases as $v^{2/3}/S_p$ increases. For both flat-top and flat-bottom unsymmetrical delta wings at constant $v^{2/3}/S_p$, $(L/D)_{MAX}$ tends to increase with leading-edge sweep and the flat-bottom configurations generally show the superior $(L/D)_{MAX}$.

The symmetrical-delta-wing results, although some data scatter is present, also tend to show the increase in $(L/D)_{MAX}$ with leading-edge sweep. (See ref. 6 for data on sharp leading-edge wings.) The trend is evident for thickness ratios of 2.5 percent and 5 percent. To show the decrease in $(L/D)_{MAX}$ due to leading-edge blunting, data for the 5-percent-thick symmetrical wing with elliptical leading edges are also included. In these wings the ellipse, generated normal to the leading edge, had its maximum thickness on the wing ridge line. A severe loss in $(L/D)_{MAX}$ occurs at lower $v^{2/3}/S_p$ (low sweep) but as the leading-edge drag is reduced at large sweep angles, the $(L/D)_{MAX}$ values are comparable to those for sharp-leading-edge wings of equal $v^{2/3}/S_p$.

The solid lines represent theoretical calculations for wedges having the same planform area and aspect ratio as the delta wings at given values of $v^{2/3}/S_p$. With this restraint the Reynolds number (based on length) for the wedges must be half that for the delta wings. The aspect ratio 0.707 corresponds to delta wings of 80° sweep whereas the aspect ratio 1.46 corresponds to delta wings of 70° sweep. Linear theory corrections were made for tip losses. The two curves cross at low values of the volume parameter because these tip losses are more severe at the lower aspect ratio. Experimental results at $M = 6.8$ for two-dimensional wedges confirm the validity of these curves.

Comparisons of the data for unsymmetrical delta wings with the data for two-dimensional wedges generally indicate that flat-bottom delta wings provide $(L/D)_{MAX}$ values equal to those for the more or less idealized wedges having the same aspect ratio and area as the delta wings.

WING-BODY COMBINATIONS

The discrete wing-body types are represented by half-cone—delta-wing combinations. These configurations were proposed by Eggers and Syvertson as a practical application wherein favorable interference benefits could be realized. (See ref. 7.) In their scheme the wing received additional lift by virtue of the superimposed flow field produced by the half cone mounted beneath the wing. Optimum configurations are then obtained when the wing sweep coincides with the cone shock so that the entire cone flow field is just contained by the wing. Experimental results at Mach numbers near 5 (see refs. 7 and 8) verified the soundness of their concept. To determine whether favorable interference benefits are actually being realized by these so-called "flat-top configurations"

it is customary to compare results with those obtained with the configuration in the inverted or "flat-bottom" position.

Latest results on these half-cone—delta-wing combinations are shown in figure 5. For these configurations various cone semivertex angles and wing leading-edge sweeps of 65° through 81° were considered. Similar models were tested at a Mach number of 6.8 in air and of 20 in helium. For clarity only the extremes in leading-edge sweep are shown here since they are typical of and show the trend of the remaining data.¹ As $v^{2/3}/s_p$ increases at constant sweep angle, the cone angles change from 3° to 9° .

The results for a Mach number of 6.8 shown at the left of figure 5, indicate a large effect of wing sweep, the higher sweeps giving the higher $(L/D)_{MAX}$ at constant volume parameter. Furthermore, the flat-top version, which is intended to take advantage of favorable interference benefits, shows superiority only at the higher sweep angles ($\Lambda = 81^\circ$). The results for a Mach number of 20 on the right show the same favorable effect of leading-edge sweep but show superiority of the flat-bottom models at all sweep angles, which indicates that no favorable interference effects are present.

From these results it is clear that $(L/D)_{MAX}$ for generic configurations is not a single function of volume parameter as has been inferred previously in references 11 and 12. Also the results in reference 13, which indicate that an essentially constant value of $(L/D)_{MAX}$ could be obtained over a wide range of $v^{2/3}/s_p$, was a specific case of the more generalized results shown in figure 5.

These results are compared with existing data from references 8, 14, and 15 in figure 6. Here the ratio of $(L/D)_{MAX}$ (flat top to flat bottom) is shown as a function of Mach number. Data for both arrow-wing and delta-wing planforms are included. The latest data at Mach numbers of 6.8 and 20 are indicated by the flagged symbols.

The overall trend of the data suggests that favorable interference benefits dissipate with Mach number and tend to disappear altogether at Mach number of about 11 and at intermediate Mach numbers certain flat-top configurations are superior while others are not. It is true that all these configurations do not represent the optimum; however, on the basis of available information, most of them might have been expected, a priori, to show some evidence of favorable interference benefits.

As far as predicting these data trends with Mach number is concerned, the simple linear theory (ref. 7), on which the original concept was based and in which only the interference effects on lift were considered, yields a trend opposite to that shown by the data. Several more sophisticated, but approximate, theories for predicting characteristics of flat-top configurations, when

¹Complete results and geometric details for all configurations are given for a Mach number of 6.86 in air in reference 9, and for a Mach number of 20 in helium in reference 10.

the leading-edge shock is attached, are available in the literature (see refs. 12 and 16) and, although they differ somewhat in details, they do yield approximately the same answers. No methods for the flat-bottom counterparts, however, have been proposed since the complex flow about the body located on the lee side of the wing poses a formidable analytical problem. In lieu of more exact methods, engineering-type calculations have been made for a configuration with a leading-edge sweep of 70° and a cone semiapex angle of 7.5° in helium flow. An outline of these calculations is given in the appendix. The results of these calculations for flat-top configurations agree with the results of the methods given in references 12 and 16. The results of these calculations are shown by the solid line in figure 6 and sensibly predict at least the data trend down to a point just short of crossover to flat-top superiority. Other calculations were made at a Mach number of 6.8 over a wide range of sweep angles, in which leading-edge shock-detachment effects were ignored, but similar results showing flat-bottom superiority were invariably obtained regardless of the sweep angle. These results are, of course, in variance with the experimental data and suggest the possibility that leading-edge shock detachment may have a significant effect on favorable interference benefits.

These same data have been recast in a form suitable for determining the effect of leading-edge shock detachment. In figure 7 the ratio of $(L/D)_{MAX}$ (flat top to flat bottom) is shown as a function of the ratio of angle of attack for shock detachment to the angle of attack for $(L/D)_{MAX}$ for the flat-bottom configuration. The optimum angle of attack for the flat-bottom configuration is used as the normalizing term, rather than the corresponding angle of attack for the flat-top configuration, because it is the meaningful term dictated by the theoretical calculations.

The plot on the left in figure 7 includes all air data from figure 6. From purely statistical considerations, the data support the suspected importance of shock detachment. The considerable dispersion in the data is believed to be due to the uncontrolled variations in Mach number, Reynolds number, and volume parameter. To eliminate variations in Mach number and Reynolds number, the data recently obtained at a Mach number of 6.8 are shown in the middle plot. These results show that favorable interference benefits are generally available only when the leading-edge shock is detached and then only in a limited range of the volume parameter. The dashed line in the data for a Mach number of 6.8 represents optimum configurations, wherein the wing leading edge and cone shock coincide. This line is included to show that even these optimum configurations do not yield favorable interference benefits unless they conform to the restriction of low values of the volume parameter. In contrast with this, the data to the right of the optimum line show that under these restrictions lower sweep angles than optimum can be used and favorable interference benefits still be obtained.

The physical reasons behind this behavior lie in the fact that with leading-edge shock detachment, high pressures from the lower wing surface can bleed around and increase the wing lee-side pressures which in turn cause a decrease in the slope of wing normal force with angle of attack. The flat-top configurations are superior under these conditions since the interference

effects cause their maximum lift-drag ratios to occur at a much lower angle of attack than their flat-bottom counterparts and they are therefore penalized to a lesser extent by the reduced normal-force slope.

These shock-detachment and low-volume-parameter criteria dictate that wings with higher leading-edge sweep angles and cones with higher fineness ratios are necessary to achieve favorable interference benefits at higher Mach numbers. At the extreme Mach numbers, however, the extreme sweep angles required may preclude the possibility of favorable interference benefits. Some evidence of this may be indicated by the group of data ($\Lambda = 81^\circ$) for a Mach number of 20 at the right in figure 7, which is seemingly at variance with the previous results. The reasons for this behavior may be the reduced lifting effectiveness of extreme leading-edge sweep or large viscous effects; however, more study will be required before this result is understood.

The effects of extreme leading-edge sweep are shown in figure 8 at a Mach number of 6.8. The ratio of $(L/D)_{MAX}$ (flat top to flat bottom) for a 5° half-cone—wing combination is shown as a function of leading-edge sweep angle. The superiority of the flat-top configuration at and near optimum sweep angles is clearly shown. At extreme sweep angles, however, the wing lifting efficiency decreases and is accompanied by high fuselage drag so that the flat-bottom version again becomes superior.

Some details of the flow about these configurations over a large Mach number range are shown in figure 9. To the left in the figure two possible shock formations about these flat-top half-cone—delta-wing combinations are indicated by experimental data at Mach numbers of about 5 and 8 taken from references 14 and 15. At angles of attack below leading-edge shock detachment a multiple shock system is formed. This multiple shock formation, however, coalesces to a single shock at the angle of attack for leading-edge shock detachment.

Pressure distributions over a hypersonically similar configuration in helium flow at a Mach number of 20 are shown at the right in figure 9. Pressure results were obtained only on the side of the wing which contained the cone. The curves for $\alpha = -4.5^\circ$ in the upper plot in the figure, therefore, represent the flat-top configuration with the half cone windward and those for $\alpha = 7^\circ$ in the lower plot represent the flat-bottom configuration with the half cone leeward. In each instance curves are shown for the half cone alone, wing alone, and wing-body combination for comparison purposes. The angles of attack chosen are those at which the respective configurations attain their maximum lift-drag ratio.

The curves for $\alpha = -4.5^\circ$, at which the leading-edge shock is still attached, from inviscid considerations, show no evidence of a multiple shock formation under the flat-top configuration. The reason for this may be that at the high value of the viscous interaction parameter $\bar{X} \approx 2$ of these tests the thick boundary layer may alter the pressure-generating surface from the intended shape to such an extent that the configuration geometric variables have lost much of their significance. Correlations based on geometric properties may, therefore, not be meaningful at the extreme Mach numbers where viscosity can

have a major influence, and applications of the hypersonic similarity laws may be grossly invalid.

The results shown in the lower right plot in figure 9 indicate that the presence of the body induces large increases in lee-side wing pressures for the flat-bottom configuration at $\alpha = 7^\circ$. The reasons for this increase are not clear. Although the leading-edge shock is still attached, from inviscid considerations, recent unpublished experiments on thin delta wings indicate that viscous interaction effects can cause premature leading-edge shock detachment. Shock detachment may also be advanced by the viscous field about the cone so that the increase in pressures could result from excessive bleed from the high-pressure undersurface. Additional work, however, is necessary to understand this result.

COMPARISON OF CONFIGURATION CLASSES

The performance of the three configuration classes is compared in figure 10 for a Mach number of 6.8. The maximum lift-drag ratio is again shown as a function of the volume parameter. The curves represent the best lift-drag ratios obtained from $3/4$ -power bodies, half cones, and rectangular and delta wings which represent merged wing-bodies. Discrete wing-body types are represented by the data points for half-cone—delta-wing combinations. Open symbols are again the flat-top orientation and solid symbols, the flat-bottom orientation. At high values of the volume parameter, wings are clearly unnecessary since the best maximum lift-drag ratios are given by the flat-bottom half bodies. At lower values of $v^{2/3}/S_p$, the flat-bottom half-cone—delta-wing combinations give results similar to those for the delta-wing types so that from these preliminary results there seems to be no significant advantage from wing-body merging. The best lift-drag ratios in this low-volume-parameter range at a Mach number of 6.8 are given by those flat-top, half-cone—delta-wing combinations which exploit the benefits of favorable interference.

EFFECTS OF GEOMETRIC VARIATIONS IN WING-BODY CONFIGURATION

The question now arises as to whether the performance of these more or less idealized half-cone—delta-wing configurations will be improved or degraded when their identity is altered to provide features which are more practical for actual applications. To attempt to answer this in a preliminary way the remaining figures (figs. 11 to 16) show the effects of varying the shapes of either the body or the wing on the wing-body characteristics. The results are for a Mach number of 6.8.

The problem of providing better volume distribution than that afforded by a cone are examined in figure 11. The $(L/D)_{MAX}$ characteristics of power-law half-body—delta-wing combinations are shown as a function of the power n . Also included are results for half of a Miele (ref. 5) minimum-drag body for a

specified volume and length. Data are shown for leading-edge sweep angles of 75° and 81° and for two values of the volume parameter. The data indicate a peak in the flat-top performance near the $3/4$ power; however, a better volume distribution than this body provides may still be wanted. The Miele body-wing arrangement has improved volume distribution, as indicated by the longitudinal cross-sectional area distributions compared with that for a cone A/A_c , in the insert plot at the right of the figure, and provides performance equal to that of the $3/4$ -power body. Similar results are seen for both values of the volume parameter.

The effect of variations in body cross-sectional shape are considered next. Results from wing-body combinations with all the bodies having the same conical area distribution are presented in figure 12 in bar-graph form. The basic cone had a half-angle of 7.01° . For reference, the cone values have been indicated in each bar. The results generally indicate that improvements in $(L/D)_{MAX}$ over the cone values are possible but in these cases the improvements are generally small.

Another commonly considered modification to basic configurations is clipping the tips of the wings to provide regions for mounting tip fins. In figure 13 the effect of variations in taper ratio on the $(L/D)_{MAX}$ for a delta- and an arrow-planform configuration is shown. The body is a 5° half-angle cone displaced from the wing by a 1° wedge. The results indicate that a significant amount of wing tip can be removed without undue penalty in $(L/D)_{MAX}$.

Some effects of departure from the optimum combination of wing and body were previously shown in figure 8. An approach such as this, however, does not include planform-shape changes such as wing-tip clipping and changes to arrow planform. Based on reasoning which led to the proposal of the flat-top configuration as a means for increasing aerodynamic efficiency the area covered by the body shock compared with exposed wing area would appear to be one of the logical parameters for assessing these configurations. Values of $(L/D)_{MAX}$ from half-cone—delta- and arrow-wing combinations of various sweep and tip clipping are shown in figure 14 as a function of the ratio of the wing area covered by the body shock within configuration limits S_{ws} to the area of the exposed wing S_w . The results appear to correlate for constant values of the volume parameter and indicate that the large penalties in $(L/D)_{MAX}$ can result if the values of S_{ws}/S_w differ significantly from 1.

An assessment of the effect of various positions of the wing on the body has been made with the wing trailing edge and body base coinciding, and the results are presented in figure 15. It should be noted that the Reynolds number for this data is 3.8×10^6 . Values of $(L/D)_{MAX}$ for a fineness-ratio-10.4 Miele minimum drag half body with various wings are shown as a function of a/L where a is the distance from the body apex to the body-wing intersection. Curves for constant $v^{2/3}/S_p$ (constant exposed wing area) are faired through the data and as a/L increases at constant $v^{2/3}/S_p$, the wing sweep decreases.

The open symbols are again flat-top configuration and the solid symbols, flat-bottom configuration.

The configuration employing a curved leading-edge wing formed to the shock shape produced by the body (the theoretically optimum conditions for favorable interference) gave an $(L/D)_{MAX}$ value which is almost the same as that produced by a configuration employing a straight wing of about 78° sweep which had the same planform area. The necessity for exactly matching the shock from curved bodies is thus seen to be of secondary importance, at least for reasonably small leading-edge diameters.

The results in figure 15 also indicate that as the wing leading edge is moved rearward, such as is found in many present conceptual studies, significant penalties in $(L/D)_{MAX}$ can be incurred. In fact, the flat-bottom body alone yields equal or better $(L/D)_{MAX}$ values than a wide range of configurations with stub wings.

Even when the wing leading edge is moved rearward from the body apex, benefits of favorable interference are still apparent; these benefits do, however, decrease with rearward movement of the wing. It is also interesting to note that the effects of leading-edge shock detachment are still evident regardless of the wing leading-edge position; for in each $v^{2/3}/S_p$ group the $(L/D)_{MAX}$ values for the flat-top and the flat-bottom configurations approach one another as the leading-edge sweep decreases.

Most of the models used in these investigations had relatively small wing leading-edge diameters of about 0.010 in., which resulted in values of d/L ranging from 0.0008 to 0.002. In actual vehicles, however, larger leading-edge diameters may be required to reduce local heating. The detrimental effect of increasing wing leading-edge diameter on $(L/D)_{MAX}$ is shown in figure 16 for a 1/2-power half-body--delta-wing combination at a Mach number of 6.8. Simple Newtonian theory corrections for leading-edge drag are seen to be generally optimistic. Similar results were also obtained in helium at a Mach number of 20 on slab wing configurations.

CONCLUDING REMARKS

Results from tests of simple body, wing, and wing-body combinations have indicated some of the factors that contribute to the attainment of high maximum lift-drag ratios at hypersonic speeds. A great deal of work needs to be done in order to understand the viscous effects produced at the higher Mach numbers. Furthermore, since preliminary tests at high Mach number indicate that leeward

surfaces can significantly affect the maximum-lift-drag-ratio characteristics of configurations, serious attention must be focused on defining the flow fields existing in this region.

Langley Research Center,
National Aeronautics and Space Administration,
Langley Station, Hampton, Va., April 6, 1965.

APPENDIX

THEORETICAL CALCULATIONS FOR HALF-CONE—DELTA-WING COMBINATIONS

The ground rules used for the $(L/D)_{MAX}$ calculations in figure 6 are:

1. Uniform two-dimensional pressure acts on the flat side of the wing (i.e., the side from which the half cone is absent), whether that side is a compression or an expansion surface.

2. On the half-cone side:

(a) The half cone always forms its own shock whether in the presence of the wing shock (compression side) or on the expansion side of the wing.

(b) The pressure and local flow direction on the wing surface between the leading edge and the half-cone shock are determined by the component of flow in an analysis normal to the leading edge on both the compression and the expansion sides.

(c) Half-cone shock position on the wing and pressures on the wing at the wing-body and wing-shock junctures are determined with the half cone in local flow on the wing surface as found from paragraph (b). (The effective cone angle varies with the local flow direction on the wing surface.)

(d) Pressure on the wing varies linearly between the wing-body and the wing-shock juncture.

(e) Pressure on the half cone 90° from the wing-body juncture is determined by the effective cone angle (i.e., $\alpha + \theta_c$ or $\alpha - \theta_c$, whichever is appropriate) in free-stream flow uninfluenced by the wing.

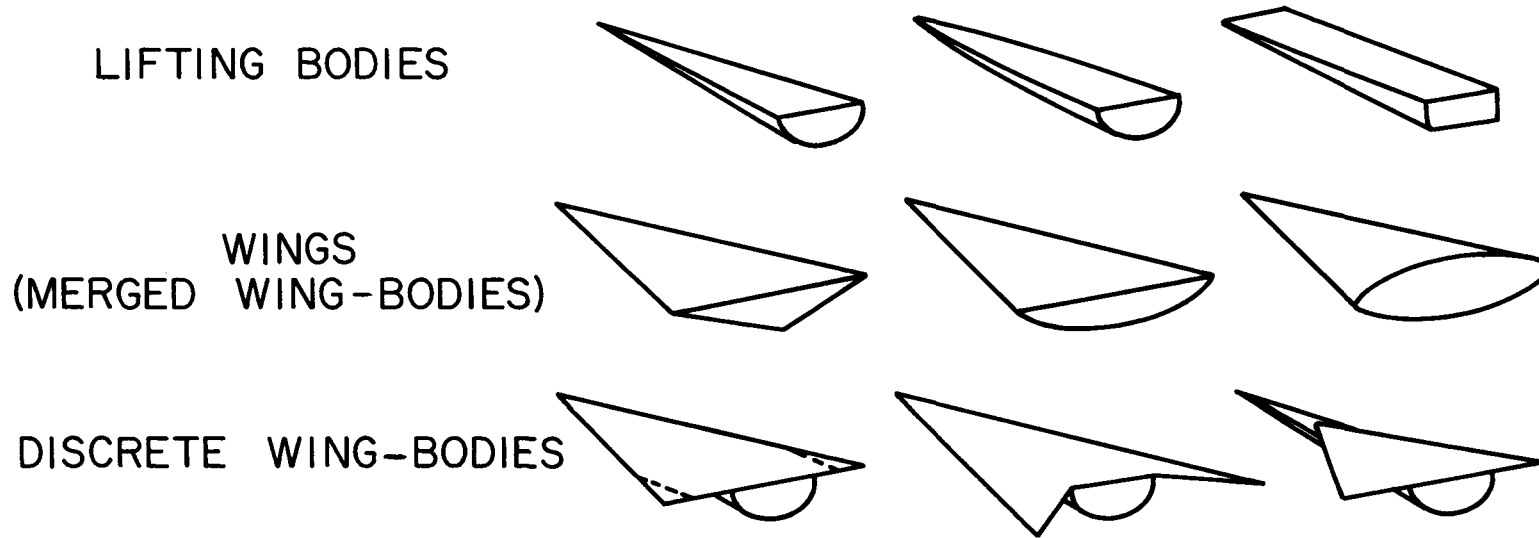
(f) Pressure on the half cone varies laterally according to the equation

$$C_{p,c} = C_{p,WB} \sin^2\phi + C_{p,o} \cos^2\phi$$

REFERENCES

1. Becker, John V.: Studies of High Lift/Drag Ratio Hypersonic Configurations. International Council of the Aeronautical Sciences, Fourth Congress, Paris - 1964, Spartan and MacMillan & Co., Ltd., 1965.
2. Bertram, Mitchel H.; and Henderson, Arthur, Jr.: Effects on Boundary-Layer Displacement and Leading-Edge Bluntness on Pressure Distribution, Skin Friction, and Heat Transfer of Bodies at Hypersonic Speeds. NACA TN 4301, 1958.
3. Bertram, Mitchel H.; and Blackstock, Thomas A.: Some Simple Solutions to the Problem of Predicting Boundary-Layer Self-Induced Pressures. NASA TN D-798, 1961.
4. White, Frank M., Jr.: Hypersonic Laminar Viscous Interactions on Inclined Flat Plates. ARS J. (Tech. Notes), vol. 32, no. 5, May 1962, pp. 780-781.
5. Miele, Angelo: Optimum Slender Body of Revolution in Newtonian Flow. Tech. Rept. No. 56, Flight Sci. Lab., Boeing Sci. Res. Lab., Apr. 1962.
6. Bertram, Mitchel H.; and McCauley, William D.: An Investigation of the Aerodynamic Characteristics of Thin Delta Wings With a Symmetrical Double-Wedge Section at a Mach Number of 6.9. NACA RM L55B14, 1955.
7. Eggers, A. J., Jr.; and Syvertson, Clarence A.: Aircraft Configurations Developing High Lift-Drag Ratios at High Supersonic Speeds. NACA RM A55L05, 1956.
8. Syvertson, Clarence A.; Gloria, Hermilo R.; and Sarabia, Michael F.: Aerodynamic Performance and Static Stability and Control of Flat-Top Hypersonic Gliders at Mach Numbers From 0.6 to 18. NACA RM A58G17, 1958.
9. Fetterman, David E.: Favorable Interference Effects on Maximum Lift-Drag Ratios of Half-Cone Delta-Wing Configurations at Mach 6.86. NASA TN D-2942, 1965.
10. Johnston, Patrick J.; Snyder, Curtis D.; and Witcofski, Robert D.: Maximum Lift-Drag Ratios of Delta-Wing-Half-Cone Combinations at a Mach Number of 20 in Helium. NASA TN D-2762, 1965.
11. McLellan, Charles H.; and Ladson, Charles L.: A Summary of the Aerodynamic Performance of Hypersonic Gliders. NASA TM X-237, 1960.
12. Goebel, T. P.; Martin, J. J.; and Boyd, J. A.: Factors Affecting Lift-Drag Ratios at Mach Numbers From 5 to 20. AIAA J., vol. 1, no. 3, Mar. 1963, pp. 640-650.
13. Bertram, Mitchel H.; Fetterman, David E., Jr.; and Henry, John R.: The Aerodynamics of Hypersonic Cruising and Boost Vehicles. Proceedings of the NASA-University Conference on the Science and Technology of Space Exploration, Vol. 2, NASA SP-11, 1962, pp. 215-234. (Also available as NASA SP-23.)

14. Mead, Harold R.; and Koch, Frank: Theoretical Prediction of Pressures in Hypersonic Flow With Special Reference to Configurations Having Attached Leading-Edge Shock - Part II. Experimental Pressure Measurements at Mach 5 and 8. ASD TR 61-60, Pt. II, U.S. Air Force, May 1962.
15. Mead, Harold R.; Koch, Frank; and Hartofilis, Stavros A.: Theoretical Prediction of Pressures in Hypersonic Flow With Special Reference to Configurations Having Attached Leading-Edge Shock - Part III. Experimental Measurements of Forces at Mach 8 and Pressures at Mach 21. ASD TR 61-60, Pt. III, U.S. Air Force, Oct. 1962. (Available from ASTIA as 291219.)
16. Savin, Raymond C.: Approximate Solutions for the Flow About Flat-Top Wing-Body Configurations at High Supersonic Airspeeds. NACA RM A58F02, 1958.



M=6.8, 9.7 AIR;
20 HELIUM

Figure 1.- Scope of program to develop high-lift-drag-ratio design principles.

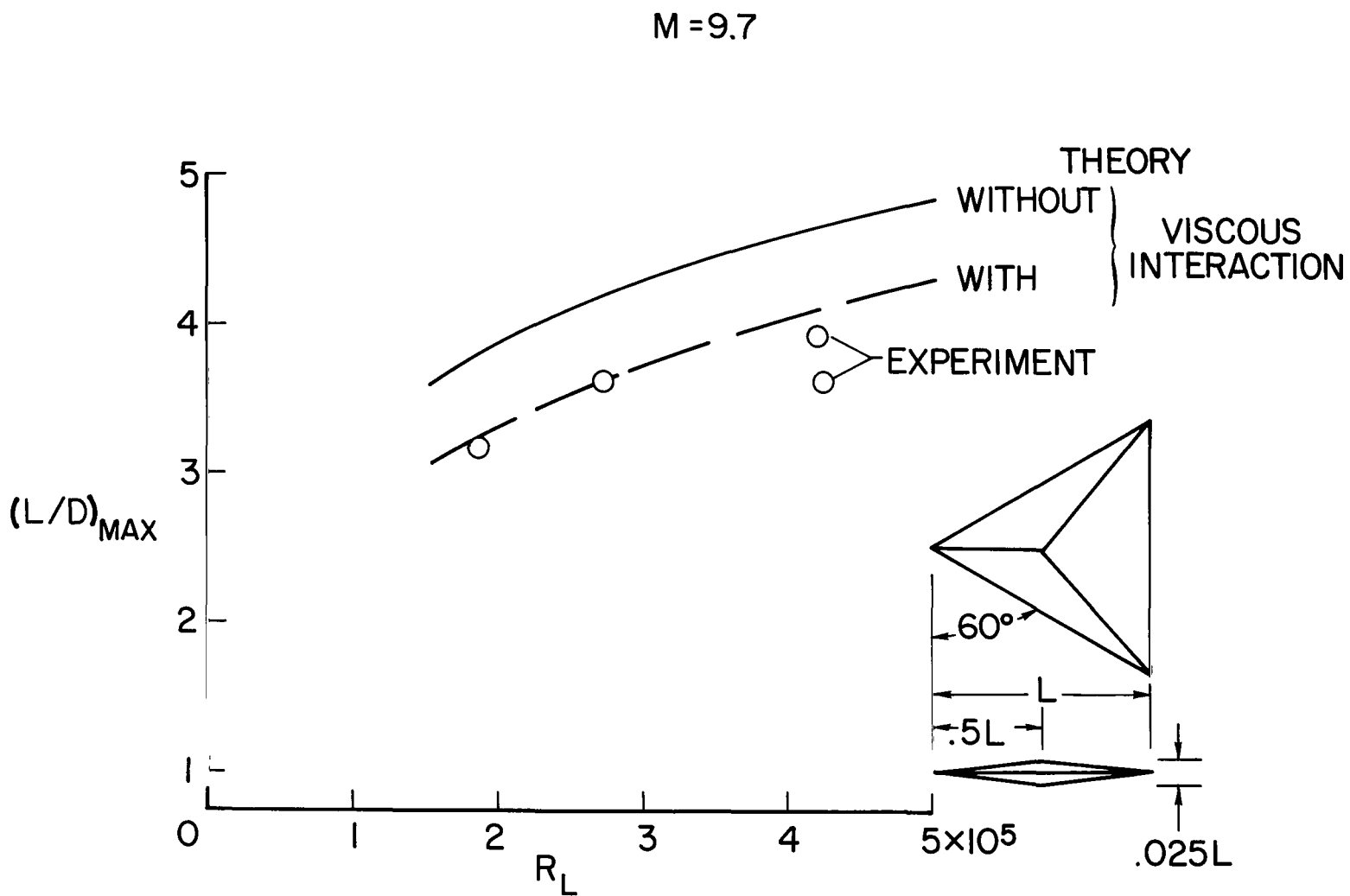


Figure 2.- Effect of viscous interaction on $(L/D)_{MAX}$.

$M = 6.8; R_L = 1.4 \times 10^6$
(AIR)

$M = 20; R_L = 3.5 \times 10^6$
(HELIUM)

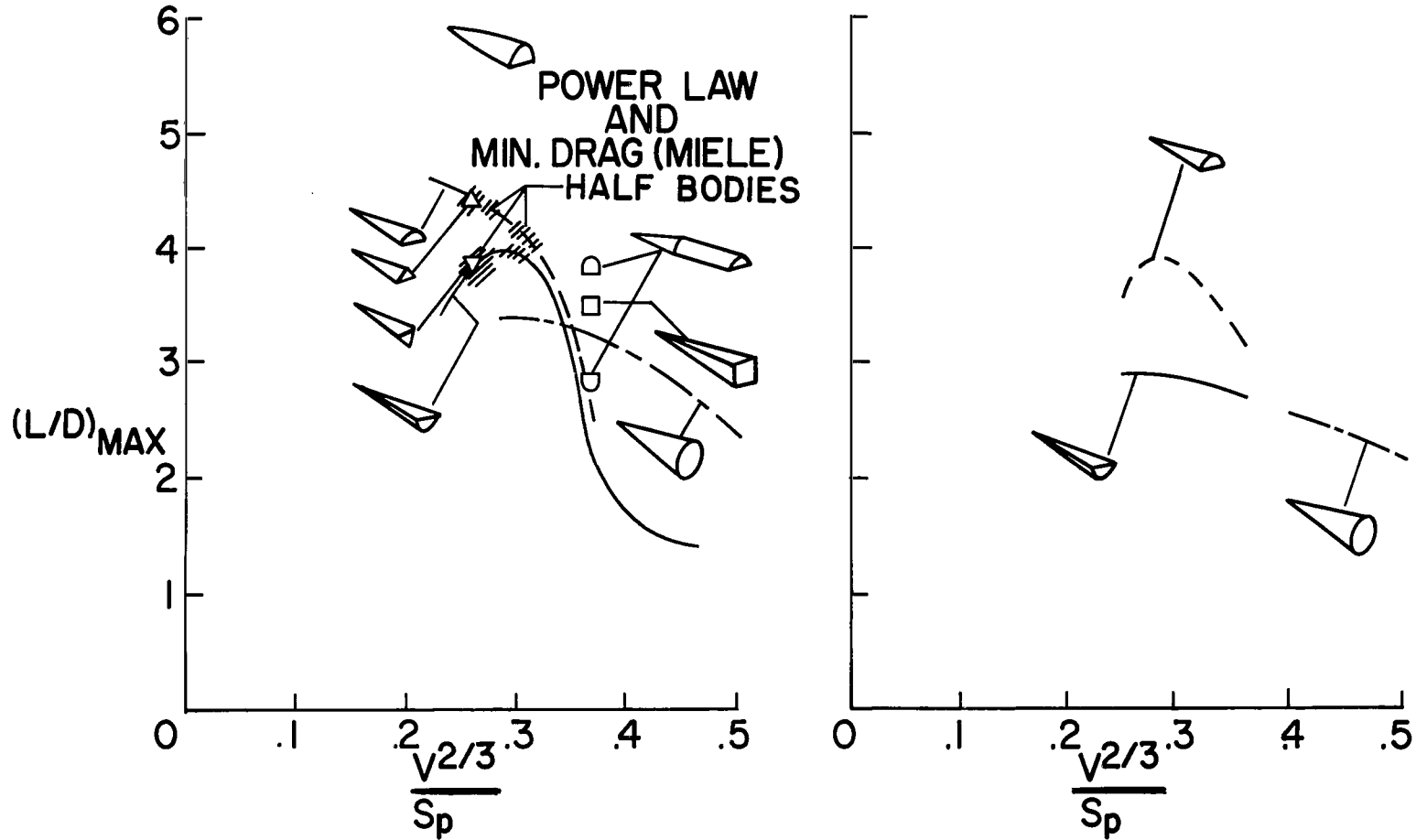


Figure 3.- Performance of pointed bodies.

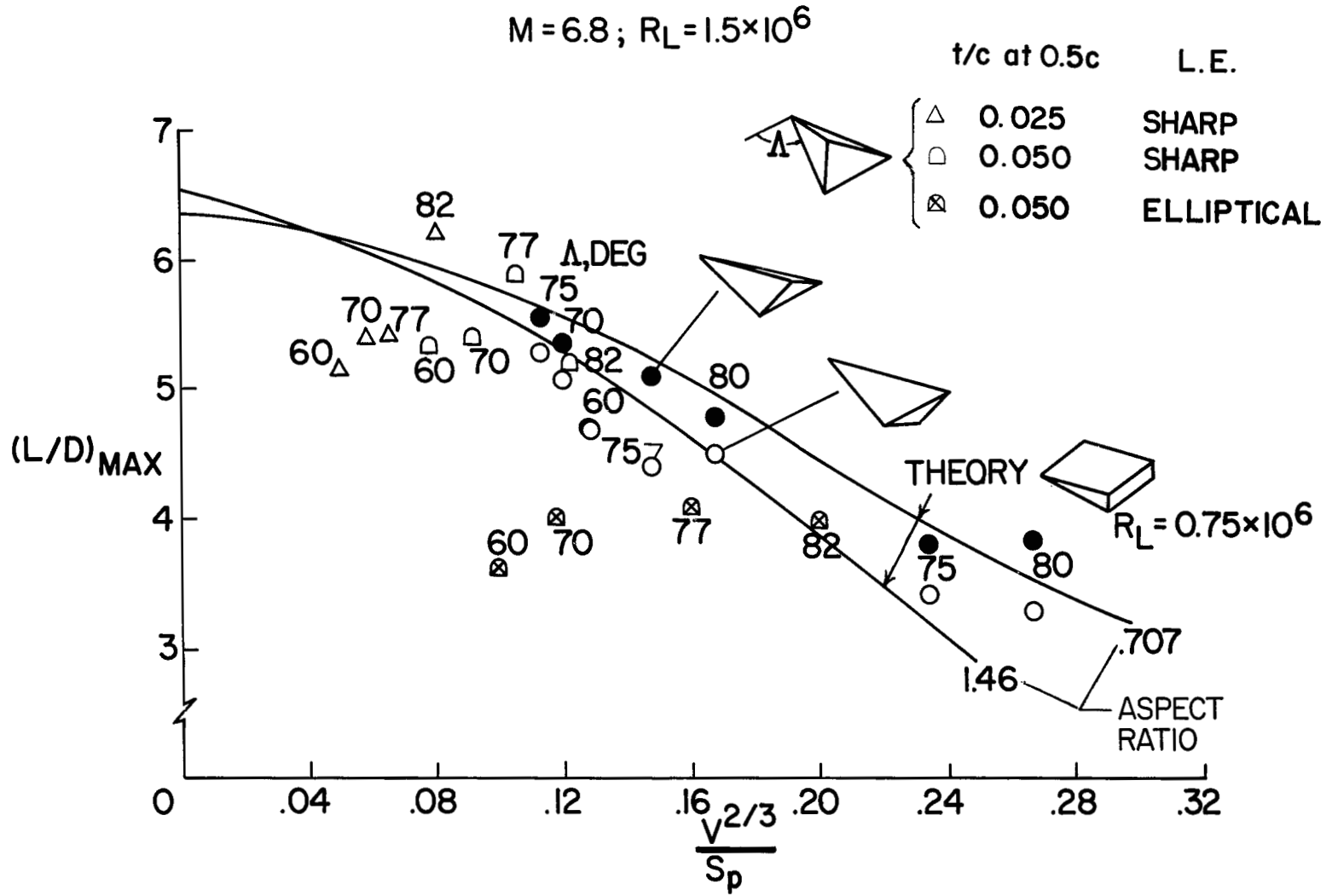


Figure 4.- Results obtained for delta wings with sharp leading edges.

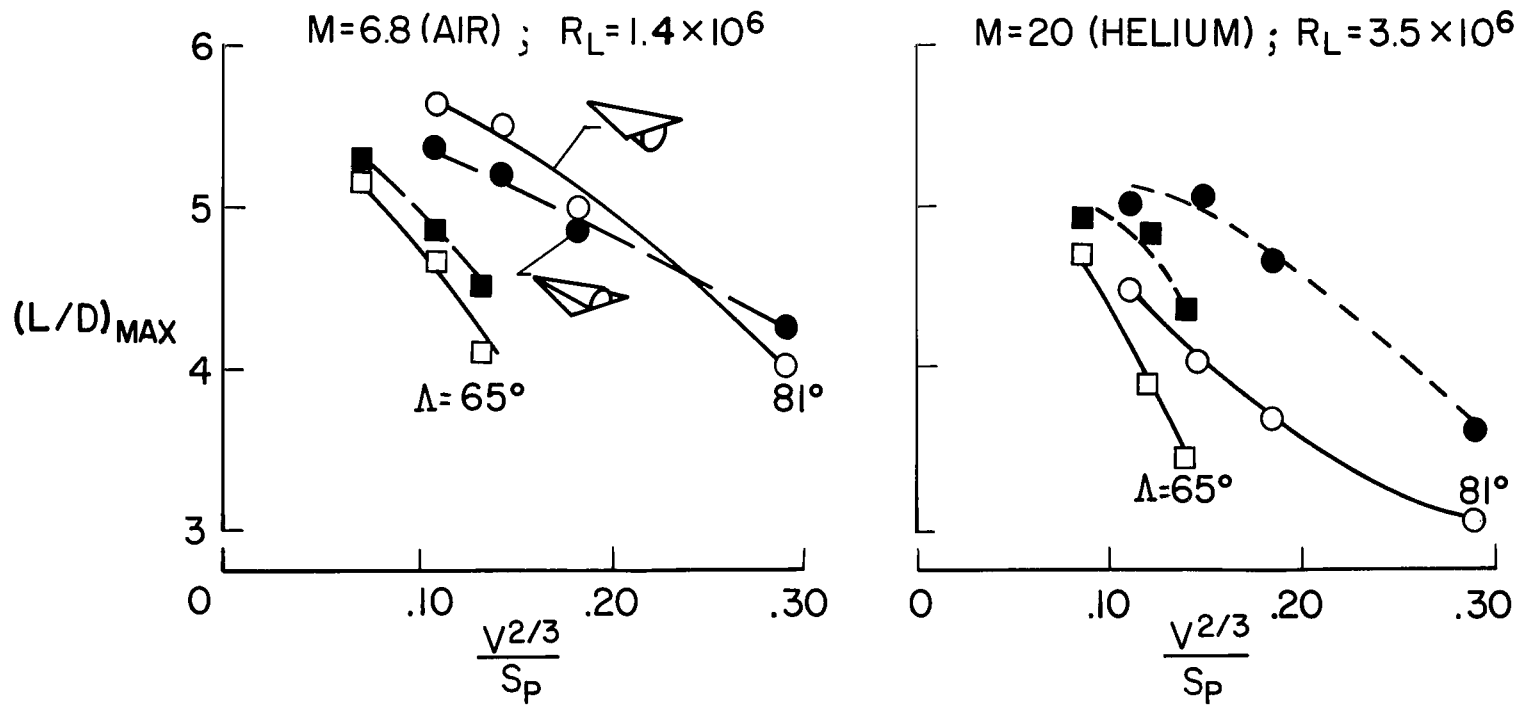
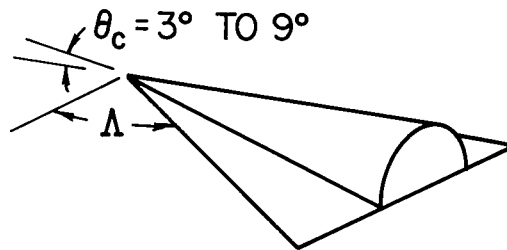


Figure 5.- Performance of half-cone--delta-wing combinations.

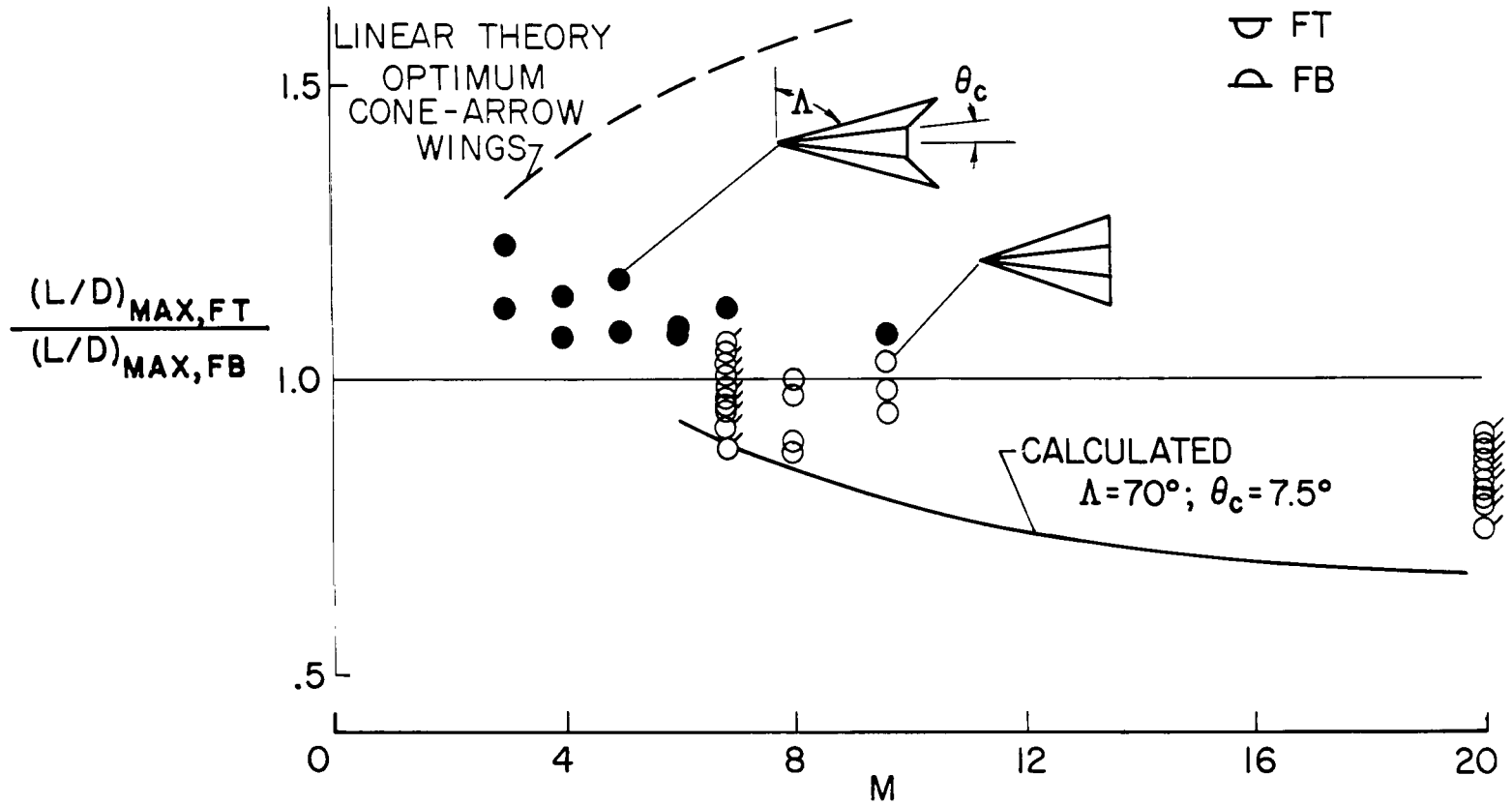


Figure 6.- Effects of Mach number on wing-body interference. Data from references 8, 14, 15, and present investigation (shown by flagged symbols).

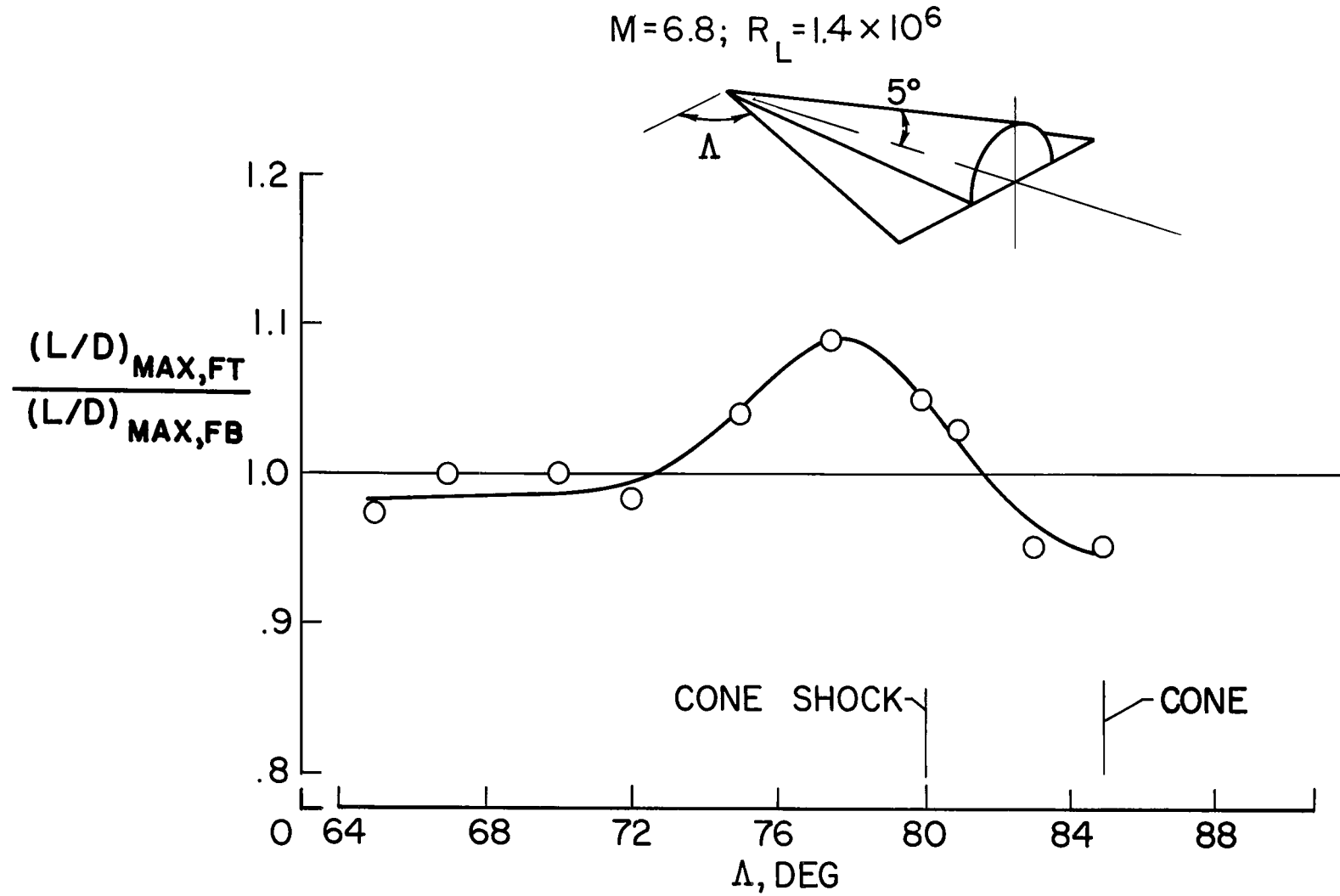


Figure 8.- Effect of wing sweep on relative performance of half-cone—delta-wing combinations.

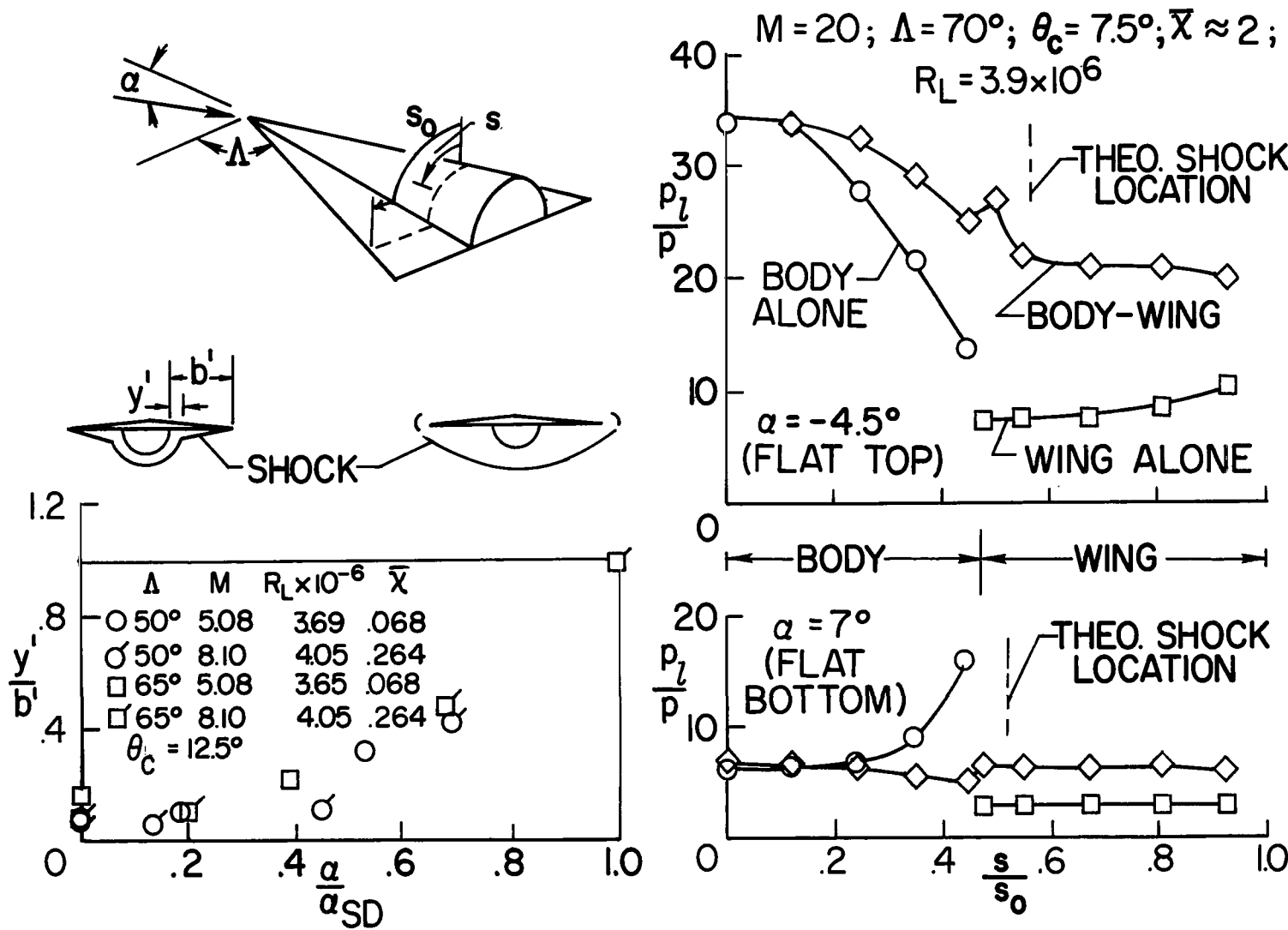


Figure 9.- Effect of angle of attack on shock position and pressure distributions. Data at Mach numbers 5.08 and 8.10 from references 14 and 15, helium data from present investigation.

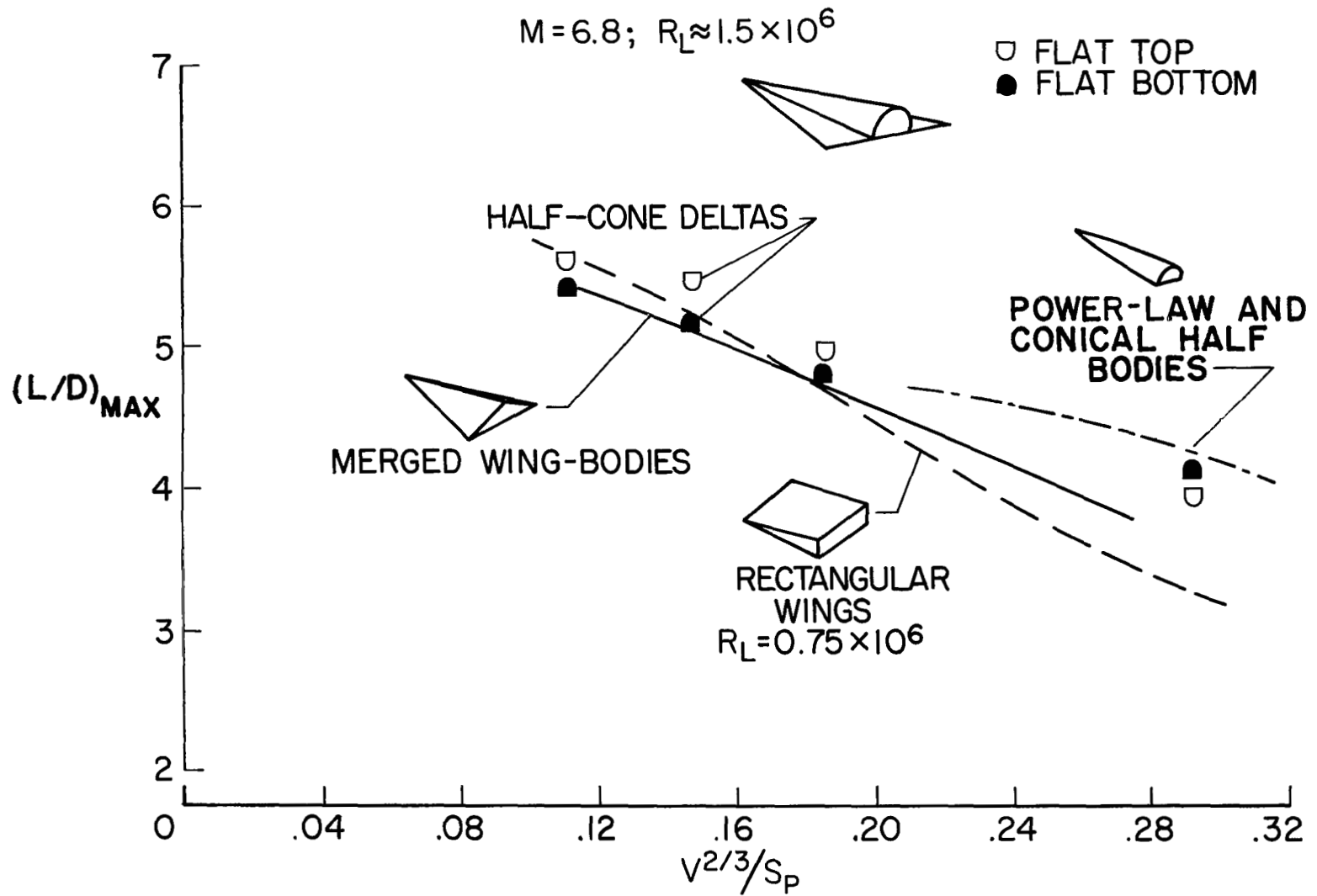


Figure 10.- Performance comparison of configurations.

$$M = 6.8; R_L = 1.5 \times 10^6$$

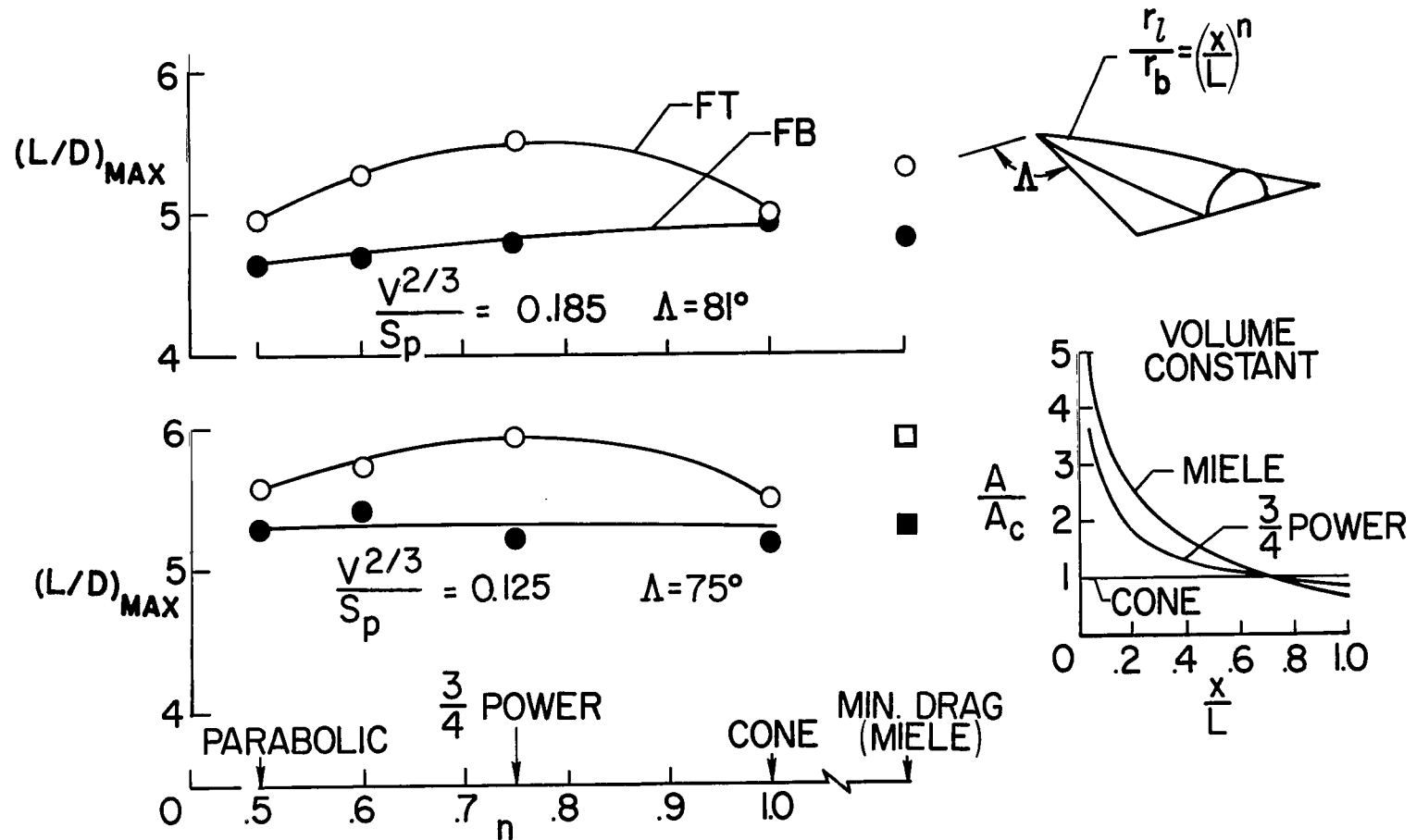


Figure 11.- Effect of body longitudinal curvature.

$$M = 6.8; R_L = 1.5 \times 10^6$$

$$\Lambda = 75^\circ$$

$$\frac{V^{2/3}}{S_p} = 0.18$$

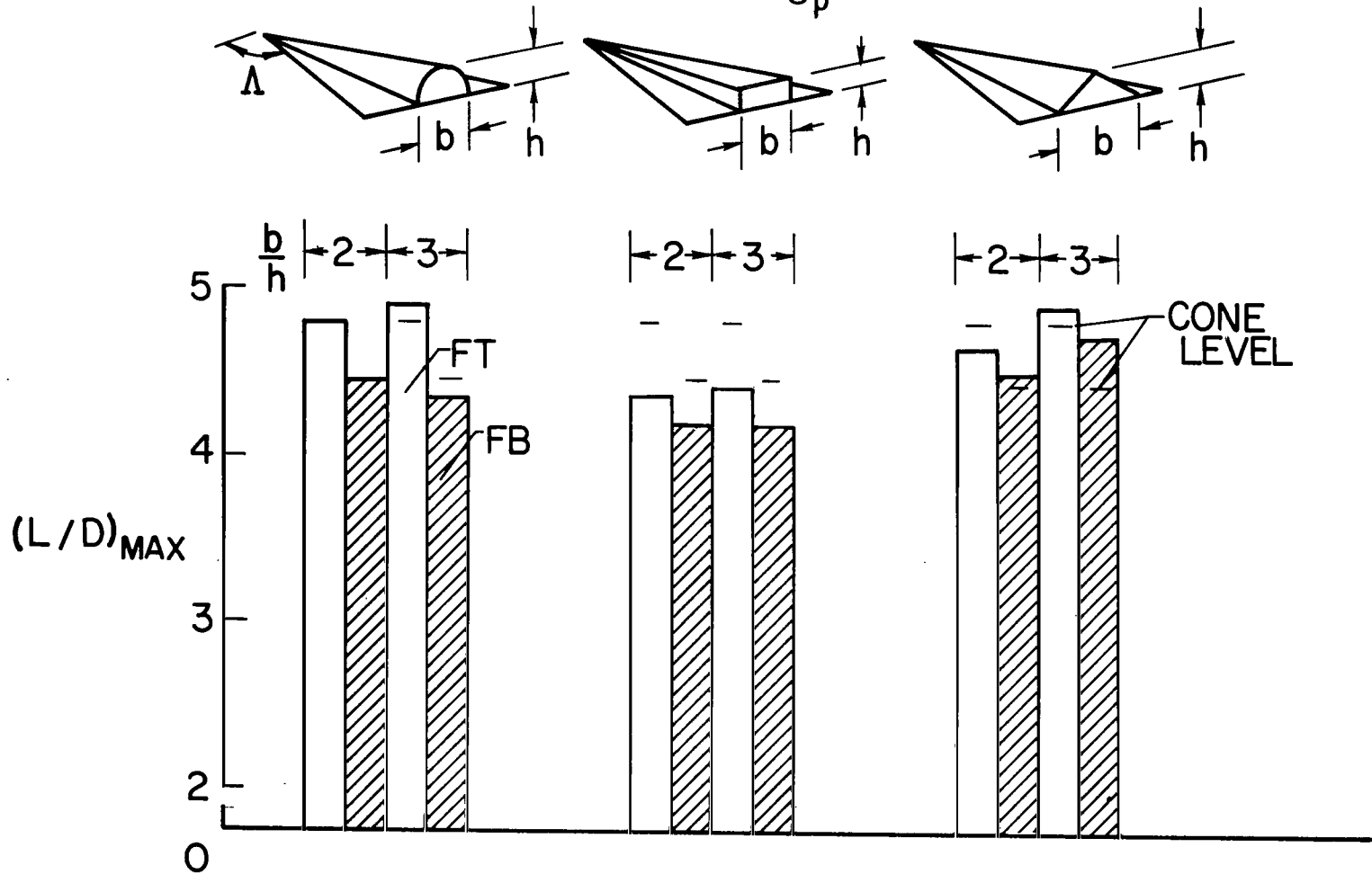


Figure 12.- Effect of body cross-section shape.

$M = 6.8; R_L = 1.5 \times 10^6; \Lambda = 77.5^\circ$

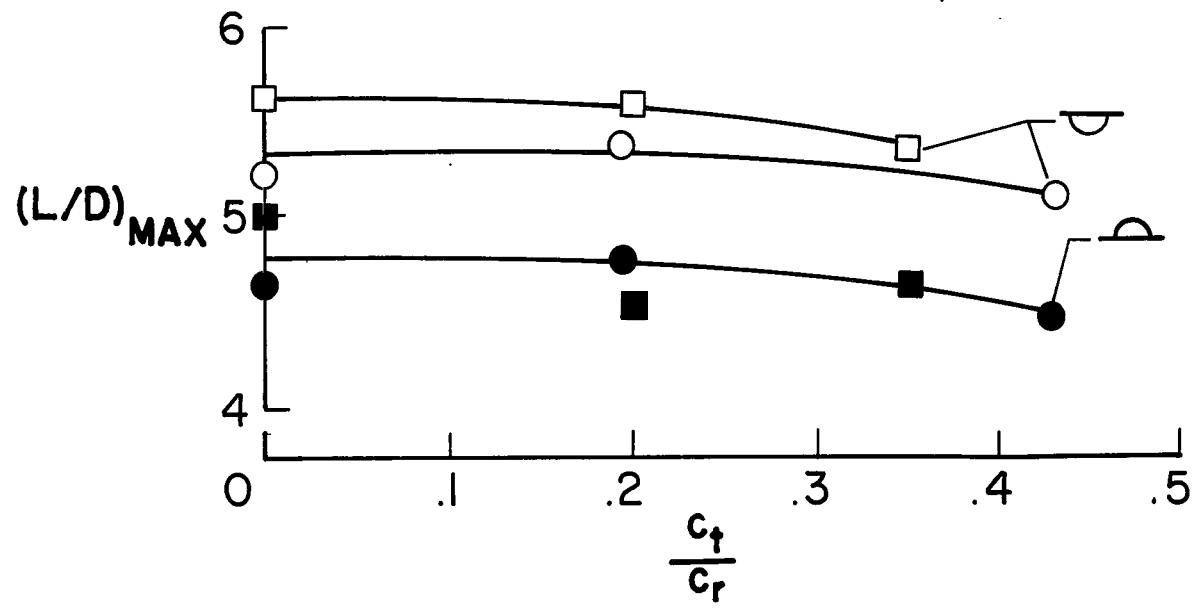
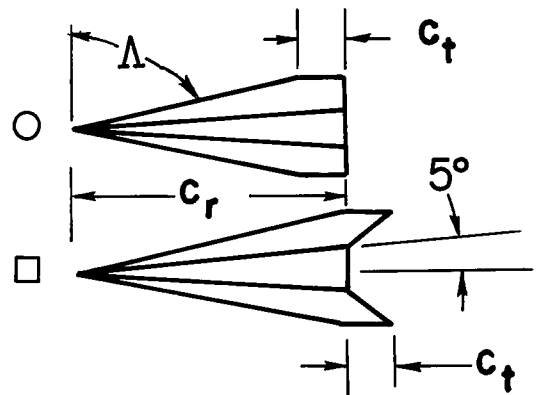


Figure 13.- Effect of wing taper ratio.

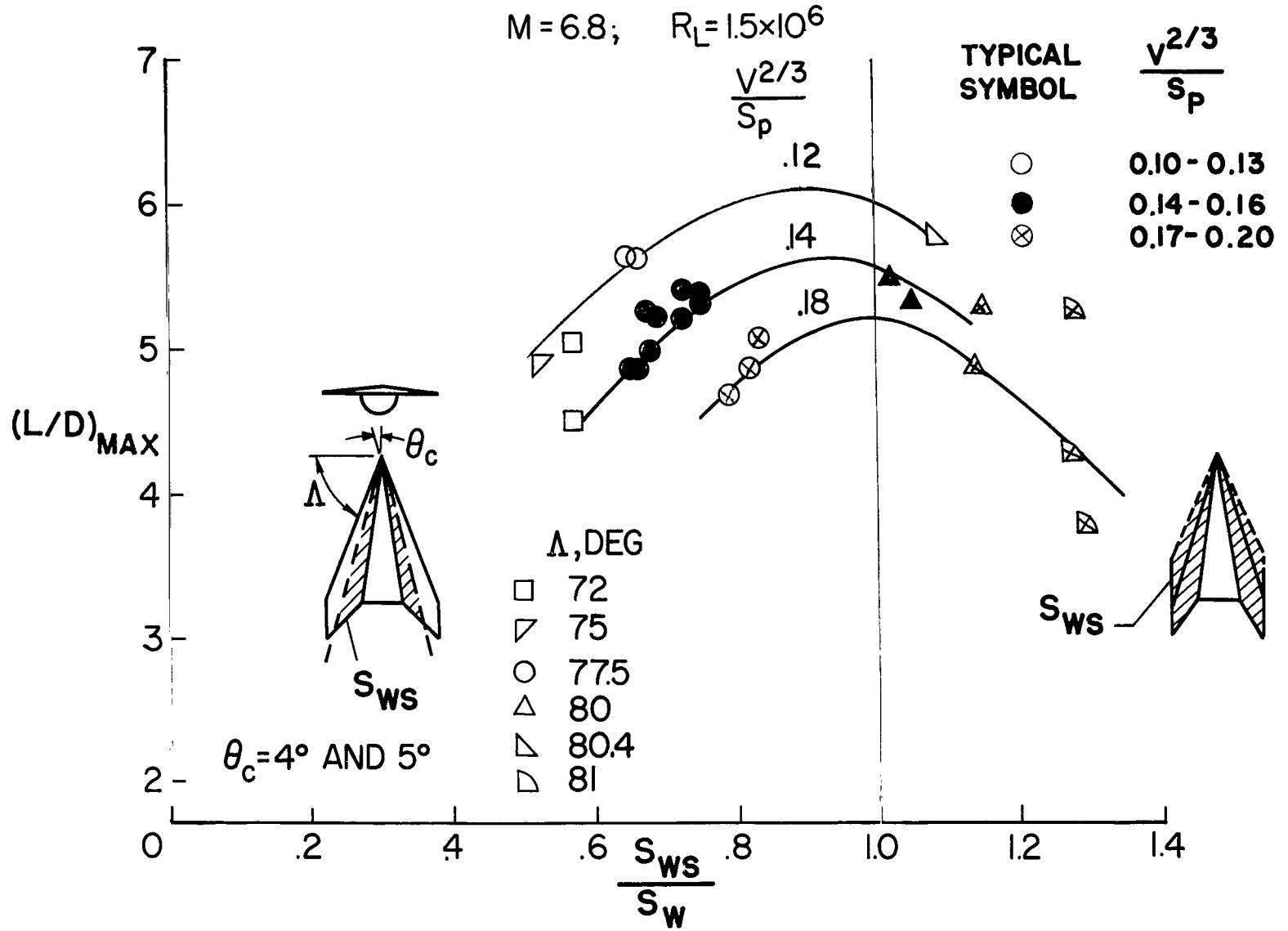


Figure 14.- Wing-planform correlation for flat-top configuration.

$M = 6.8; R_L = 3.8 \times 10^6$

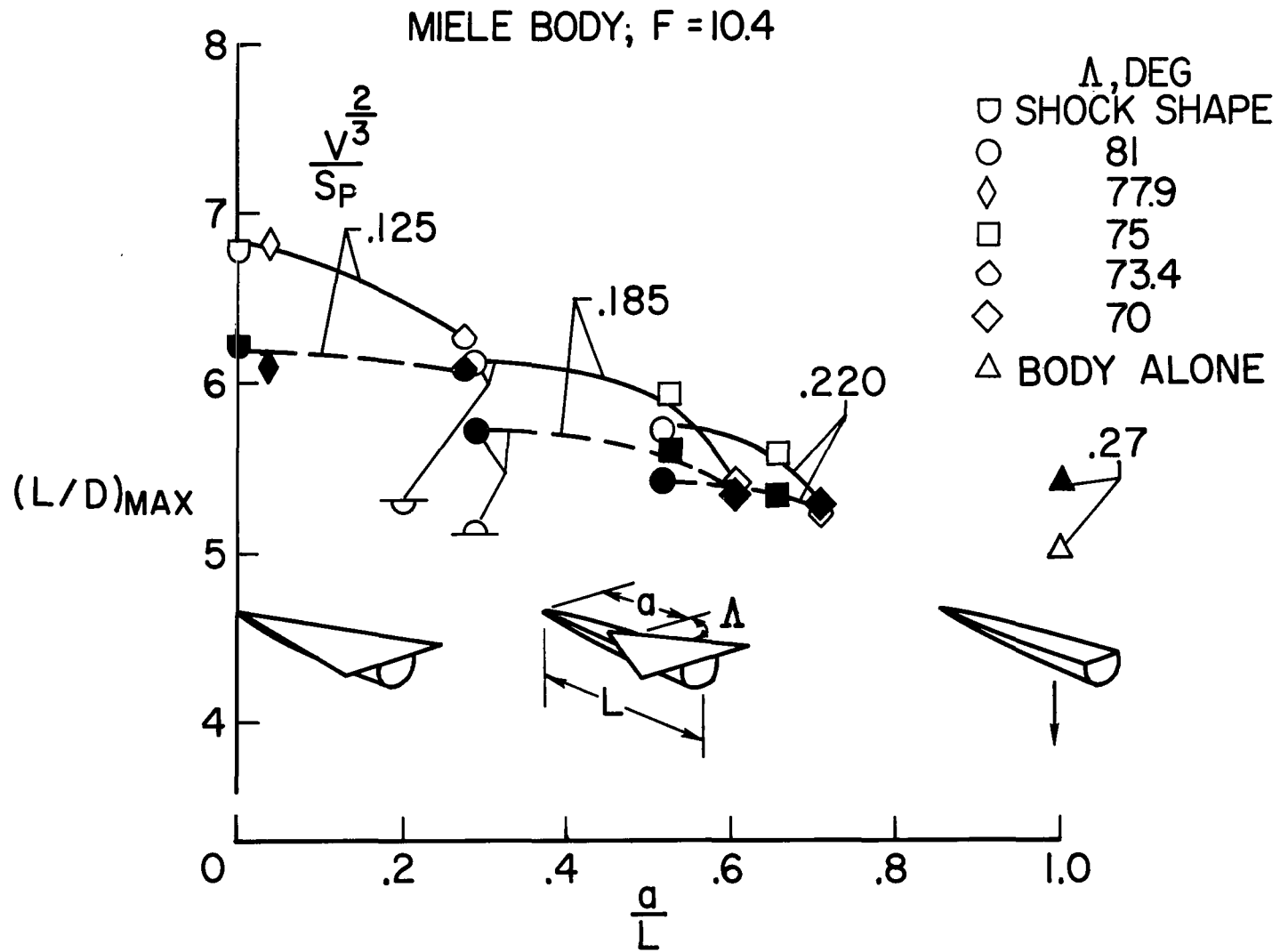


Figure 15.- Effect of wing position.

$$M=6.8; R_L=3.8 \times 10^6$$

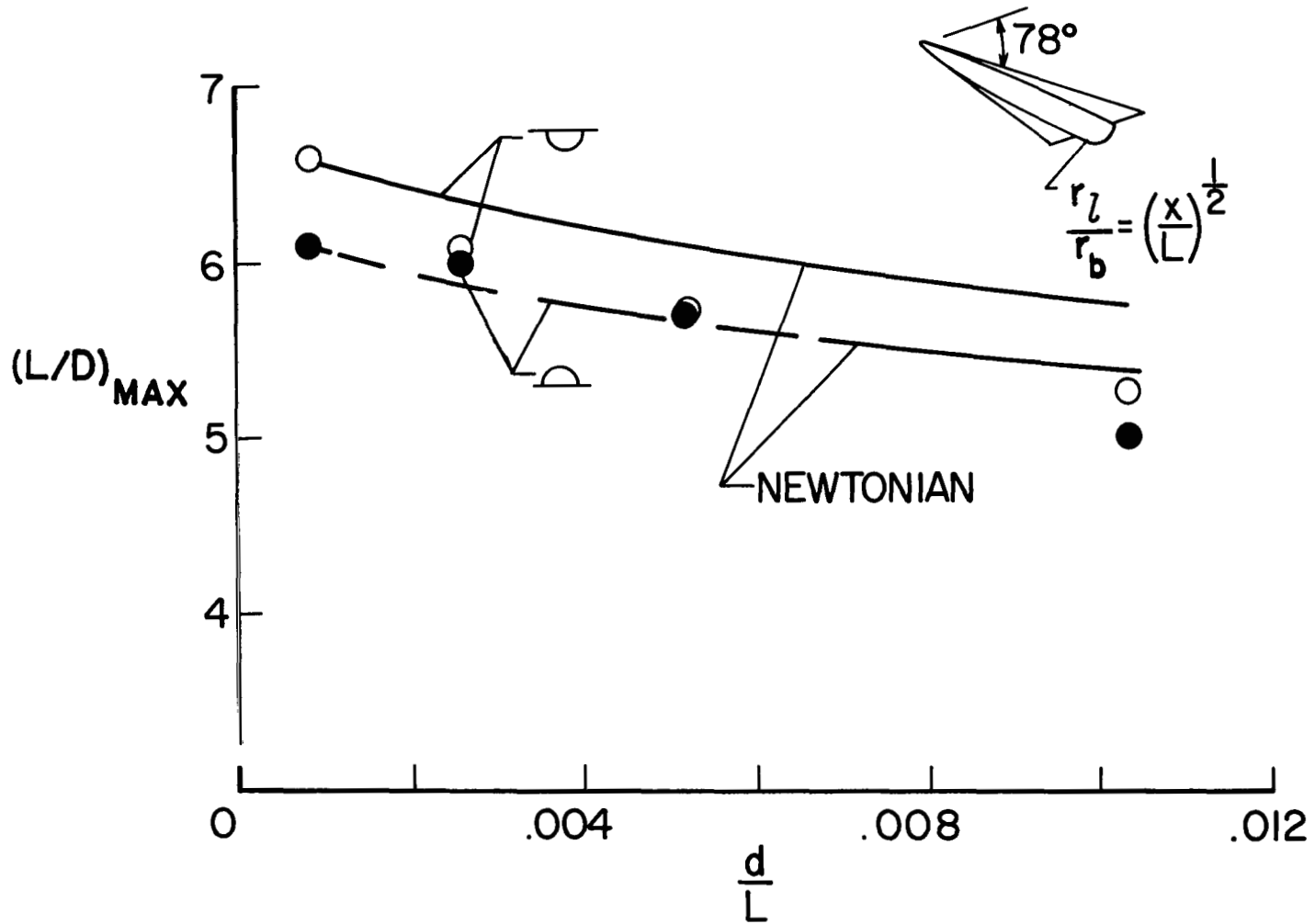


Figure 16.- Effect of leading-edge diameter on $(L/D)_{MAX}$.